mathematics

MDPI

Article

The Role of a Two-Phase Region in Directional Crystallization of Binary Liquids

Dmitri V. Alexandrov [1], Irina V. Alexandrova [1], Alexander A. Ivanov [1] and Liubov V. Toropova [2,3,*]

[1] Laboratory of Multi-Scale Mathematical Modeling, Department of Theoretical and Mathematical Physics, Ural Federal University, Lenin Ave., 51, Ekaterinburg 620000, Russia; dmitri.alexandrov@urfu.ru (D.V.A.); irina.alexanderova@urfu.ru (I.V.A.); alexandr.a.ivanov@bk.ru (A.A.I.)
[2] Laboratory of Mathematical Modeling of Physical and Chemical Processes in Multiphase Media, Ural Federal University, Ekaterinburg 620000, Russia
[3] Otto-Schott-Institut für Materialforschung, Friedrich-Schiller-Universität-Jena, 07743 Jena, Germany
* Correspondence: liubov.toropova@uni-jena.de

Abstract: Motivated by the widespread occurrence of directional crystallization in nature, laboratory experiments and industrial facilities, we consider how a two-phase (mushy) region filled simultaneously with liquid and solid material influences the process and changes the solute concentration in both the phases. A mushy layer arising as a result of constitutional supercooling in binary liquids drastically changes all process parameters in comparison with the frequently used approximation of a macroscopically planar phase interface. The heat and mass transfer problem with a moving mushy region is replaced by the equivalent model with a discontinuity interface that divides the liquid and solid phases and inherits the properties of a mushy layer. Analytical solutions that describe both crystallization modes with a planar phase interface and discontinuity interface (representing a mushy layer) are constructed for the steady-state and self-similar conditions. The switching time of the crystallization model with a planar phase interface to the model with a two-phase layer is determined. Our calculations, based on analytical solutions, show that the presence of a mushy layer can change the solute concentration in liquid and solid phases to a few tens of percent as compared to the planar interface model. This explains the importance of accounting for the two-phase region when describing the crystallization of supercooled binary liquids.

Keywords: phase transformation; heat and mass transfer; two-phase layer; moving boundary problem; binary system; constitutional supercooling

MSC: 82C26

Citation: Alexandrov, D.V.; Alexandrova, I.V.; Ivanov, A.A.; Toropova, L.V. The Role of a Two-Phase Region in Directional Crystallization of Binary Liquids . *Mathematics* **2024**, *12*, 2178. https://doi.org/10.3390/math12142178

Academic Editor: Andrey Jivkov

Received: 6 June 2024
Revised: 3 July 2024
Accepted: 7 July 2024
Published: 11 July 2024

1. Introduction

The directional crystallization of melts and solutions is often studied under the assumption of a sufficiently smooth interface (crystallization front) by means of the classical Stefan problem [1,2]. For a binary melt or solution, this problem reduces to solving the equations of heat conduction and solute diffusion in the regions occupied by liquid and solid phases at certain initial and boundary conditions given at the outer surfaces of these regions and at the moving phase interface. If the exchange kinetics of molecules or atoms between the liquid and solid phases do not limit the use of such an approach, the governing system of equations and boundary conditions takes the form of

$$\begin{gathered}\frac{\partial T_l}{\partial t} = a_l \nabla^2 T_l, \quad \frac{\partial C_l}{\partial t} = D_l \nabla^2 C_l, \quad \text{liquid phase,} \\ \frac{\partial T_s}{\partial t} = a_s \nabla^2 T_s, \quad \frac{\partial C_s}{\partial t} = D_s \nabla^2 T_s, \quad \text{solid phase,} \\ \left.\begin{array}{l} T_l = T_s = T_0 - mC_l, \quad C_s = kC_l, \\ \lambda_s \mathbf{n} \nabla T_s - \lambda_l \mathbf{n} \nabla T_l = \rho L u, \\ D_s \mathbf{n} \nabla C_s - D_l \mathbf{n} \nabla C_l = (1-k) C_l u \end{array}\right\} \text{phase interface.}\end{gathered} \tag{1}$$

In the general case, initial and boundary conditions at the outer surfaces specifying the phase transition process must also be added to this system. Here, T and C stand for the temperature and solute concentration, a and D are the temperature diffusivity and solute diffusion coefficient, t is the time, T_0 is the crystallization temperature of pure melt, m and k are the equilibrium liquidus slope and partition coefficient, λ is the thermal conductivity, ρ is the density of solid material, L is the latent heat parameter, u is the normal velocity of the phase interface (crystallization velocity), $\mathbf{n}$ is the normal vector to the phase interface directed to the liquid material and subscripts l and s correspond to the physical values in the liquid and solid, respectively. The first and second lines of Equation (1) describe the thermal and concentration fields in the liquid and solid phases, respectively, whereas the third line defines the boundary conditions at the phase interface. The first of them represents the liquidus line equation following from the phase diagram, the second boundary condition stands for the constant ratio of solute concentrations $C_s/C_l = k$ at the phase interface and the third and fourth boundary conditions are the heat and mass balances at the phase interface. Equation (1) contains all the conditions at the phase interface necessary for the correct formulation of the boundary value problem in liquid and solid phases and an additional condition for the determination of unknown crystallization velocity u. If we neglect, as is usually the case (and as is considered below), the solute diffusion in solid material, we should omit the diffusion equation in the solid and formally put $D_s = 0$.

If the inequality $T_l > T_0 - mC_l$ is fulfilled throughout the process at all points in the liquid (except the interphase boundary), the aforementioned problem adequately describes the physical process of directional crystallization. However, under certain conditions, due to solute redistribution ahead of the moving phase interface, a region with a lower melt temperature than the liquidus temperature appears, i.e., constitutional supercooling takes place [2,3]. In this case, the aforementioned problem describes the crystallization process approximately if the development of dendrites and the formation of crystal nuclei by fluctuations or on impurities can be neglected at the phase interface [4–7]. Hence, the above conditions may be fulfilled for high-purity melts with relatively retarded nucleation kinetics if the morphological instability of the crystallization front leads to the development of cellular structures rather than dendrites. This is the case for many semiconductor and some metallic melts, where the experimentally observed supercooling can reach dozens of degrees [8].

Generally speaking, a transition two-phase (mushy) layer filled with both discrete crystals and dendritic branches forms in the region of constitutional supercooling [2,9–11] (see Figure 1). The solid phase concentration in this zone is ultimately determined by the ratio between the characteristic times of crystallization front motion and the growth of individual dendrites and crystals. Therefore, a detailed analysis of the constitutional supercooling region requires a simultaneous investigation of the nonlinear equations of heat conduction and impurity diffusion in a heterogeneous, topologically complex medium and kinetic equations describing the occurrence and evolution of solid phase elements [12–16]. Significant simplification is achieved in the limiting cases where the solid phase elements in the two-phase region appear sufficiently rapidly, i.e., the structure of this region nearly has thermodynamically equilibrium [17–21]. Such situations occur for real aqueous solutions, melts of steels and, in general, for melts with foreign catalysts of crystallization where the observed supercoolings can be quite small [22–26]. However, even in this case, it is necessary to solve the very complex problems of nonlinear heat and mass transfer equations, the analytical solution of which can only be constructed using a number of simplifying assumptions [19–21,27,28]. Note that the mathematical model becomes more complex when crystal-

lization of a multicomponent system occurs (two or more mushy regions are formed [29–31]) or when intense nucleation and growth of crystals within a two-phase region take place (non-equilibrium crystallization with a mushy region [32,33]). Also, an important case is the crystallization of the two-phase region at the Earth's core, where the melt convection and pressure dependence of the phase diagram have to be taken into account [34,35].

The main concept of this paper is to construct a universal method for the analysis of such problems, abandoning a detailed consideration of the two-phase zone structure and replacing it by a geometric discontinuity surface, as has been performed many times in various fields of applied physics. This technique makes sense only when the two-phase (mushy) layer thickness is much smaller than the linear scales of the process under study.

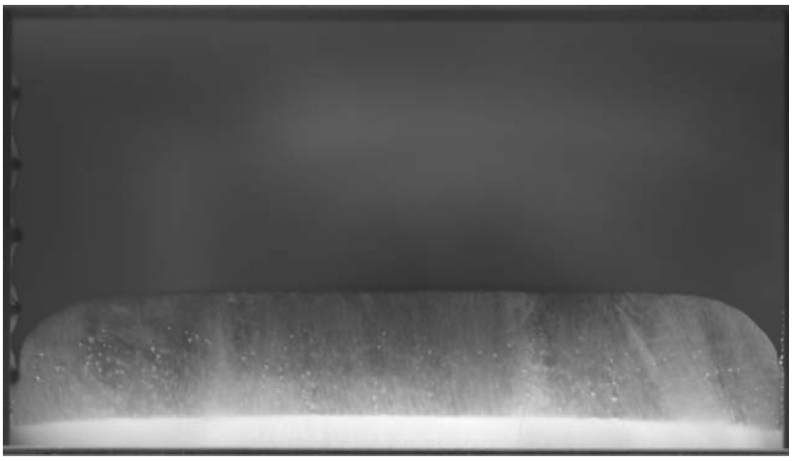

Figure 1. Mushy layer of NaCl solution is above the eutectic (white layer at the bottom). Thermistors with 1 cm spacing can be seen on the left [11], reproduced with permission.

2. The Effect of Constitutional Supercooling and the Model of Mushy Layer Crystallization with a Discontinuity Interface

Let us first consider a uni-directional crystallization process with a constant velocity u along the spatial direction y (a planar phase interface is at $y = 0$) neglecting the mushy layer formation and solute diffusion in the solid phase (Figure 2a). Introducing the solute concentration C_∞ far from the phase interface (at $y \to \infty$), let us write out the steady-state solute distribution in the liquid following from Equation (1):

$$C_l = C_\infty \left[1 + \frac{1-k}{k} \exp\left(-\frac{uy}{D_l} \right) \right], \quad y > 0. \tag{2}$$

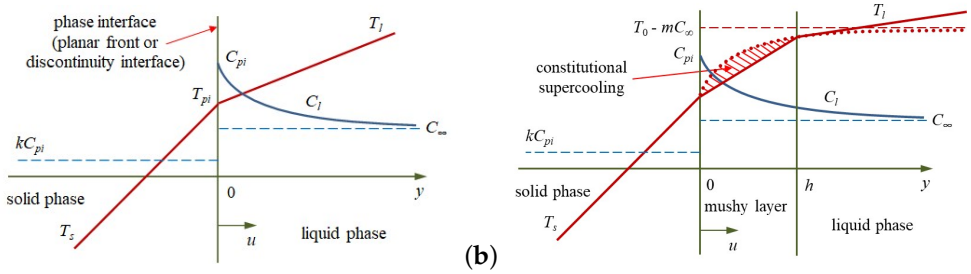

Figure 2. A scheme of directional crystallization with a planar front or discontinuity interface (**a**) and a region of constitutional supercooling (mushy layer) (**b**). The solid phase solidifies with a velocity u along the spatial axis y whose origin is at the liquid–solid interface (**a**) and the mushy layer–solid phase interface (**b**). The mushy layer of thickness h arises as a result of constitutional supercooling (**b**).

The temperature fields in the liquid and solid phases at small distances from the phase interface can be regarded as linear functions of y, i.e.,

$$T_l(y) = T_{pi} + g_l y,\ y > 0,\ \ T_s(y) = T_{pi} + g_s y,\ y < 0, \tag{3}$$

where g_l and g_s are the fixed temperature gradients, and the phase interface temperature T_{pi} is given by $T_{pi} = T_0 - mC_{pi} = T_0 - mC_\infty/k$.

The constitutional supercooling (shaded region in Figure 2b) appears when the concentration gradient multiplied by the liquidus slope exceeds the temperature gradient, i.e.,

$$-m\frac{\partial C_l}{\partial y} > \frac{\partial T_l}{\partial y} = g_l. \tag{4}$$

Combining (2) and (4), we obtain the condition of constitutional supercooling at the phase interface $y = 0$:

$$\frac{(1-k)mC_\infty u}{kD_l} > g_l. \tag{5}$$

As this takes place, the thickness $y = h$ of the supercooled layer is defined by the equality $T_0 - mC_l(h) = T_l(h)$ (see Figure 2b), which reads as

$$\exp\left(-\frac{uh}{D_l}\right) = 1 - \frac{kg_l h}{(1-k)mC_\infty}. \tag{6}$$

The numerical solution of this equation determines h, which is shown in Figure 3, in accordance with the material parameters from Table 1 for Ti-Al and Al-B melts. As can easily be seen, the thickness h of the supercooled layer increases with the increase in the phase interface (crystallization) velocity u and the decrease in the temperature gradient g_l. In addition, for the Al-B melt ($k = 0.14$), the lower crystallization velocity u leads to a higher thickness h than for the Ti-Al melt ($k = 0.86$) due to higher impurity displacement by the phase interface ($-m\partial C_l/\partial y$ for the Al-B melt is higher than for the Ti-Al melt, and, therefore, the thickness h of its supercooled region is also higher).

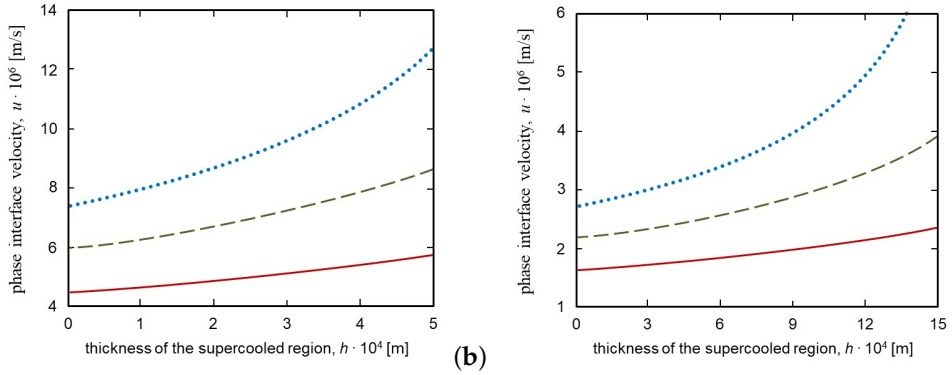

Figure 3. Crystallization velocity u as a function of supercooled layer thickness h for Ti-Al (**a**) and Al-B (**b**) melts (material parameters are listed in Table 1) at (**a**) $g_l = 6 \times 10^3$ K/m (solid line), $g_l = 8 \times 10^3$ K/m (dashed line), $g_l = 10^4$ K/m (dotted line); (**b**) $g_l = 6 \times 10^4$ K/m (solid line), $g_l = 8 \times 10^4$ K/m (dashed line), $g_l = 10^3$ K/m (dotted line).

Let us now consider the opposite case, where a quasi-equilibrium mushy layer arises as a result of constitutional supercooling. In this case, the equality $T(y) = T_0 - mC(y)$ is approximately fulfilled at any point of the mushy layer (within the interval $0 < y < h$), where $T(y)$ and $C(y)$ are the temperature and solute concentration in the mushy layer. The physical meaning of this equality is clear from the scheme shown in Figure 2b. From this scheme and the obvious requirement for continuity of the heat and mass fluxes at

the interface $y = h$ between the two-phase layer and the liquid phase, it follows that the following relation should be fulfilled:

$$-m\mathbf{n}(\nabla C_l)_{y=h} = \mathbf{n}(\nabla T_l)_{y=0}. \tag{7}$$

This condition accounts for the mushy layer and replaces the last condition in the frontal model (1).

Table 1. Material parameters of Ti-Al and Al-B melts.

Parameter	Ti-5 at.%Al Refs. [36–38]	Al-5 at.%B Refs. [39,40]
Diffusion coefficient, D_l, m^2 s^{-1}	5.27×10^{-9}	4.4×10^{-9}
Temperature diffusivity in liquid, a_l, m^2 s^{-1}	7.5×10^{-6}	8.5×10^{-6}
Temperature diffusivity in solid, a_s, m^2 s^{-1}	6.5×10^{-6}	3.1×10^{-6}
Thermal conductivity in liquid, λ_l, J m^{-1}s^{-1} K^{-1}	29.22	89.3
Thermal conductivity in solid, λ_s, J m^{-1}s^{-1} K^{-1}	39.019	185.5
Density of solid phase, ρ, kg m^{-3}	4.002×10^3	2.6×10^3
Latent heat parameter, L, J kg^{-1}	3.37×10^5	8.124×10^6
Partition coefficient, k	0.86	0.14
Liquidus slope, m, K at.%$^{-1}$	8.78	5.3
Nominal concentration, C_∞, at.%	5	5
Crystallization temperature of pure melt, T_0, K	1748	933.45
Far-field temperature in liquid, $T_{l\infty}$, K	2300	1350
Far-field temperature in solid, $T_{s\infty}$, K	900	700

The temperature jump ΔT in the mushy layer is connected with temperatures at both sides of this region as

$$\Delta T = T_l(h) - T_s(0), \;\; \Delta T = \int_0^h \frac{\partial T}{\partial y} dy. \tag{8}$$

In addition, the heat balance condition (the third boundary condition in model (1)) should be satisfied at $y = 0$.

If a mushy layer is small enough (see h in Figure 3) and the temperature jump across this layer is insignificant (temperature gradients g_l and g_s are not vastly different), it is possible to change the mushy layer by a discontinuity interface $y = 0$ ($h \to 0$). An important point is that the new boundary condition (7) at this discontinuity interface reflects the properties of the mushy layer being replaced by it. As a result, we arrive at the following model:

$$\begin{gathered} \frac{\partial T_l}{\partial t} = a_l \nabla^2 T_l, \;\; \frac{\partial C_l}{\partial t} = D_l \nabla^2 C_l, \;\; \text{liquid phase}, \\ \frac{\partial T_s}{\partial t} = a_s \nabla^2 T_s, \;\; \frac{\partial C_s}{\partial t} = D_s \nabla^2 T_s, \;\; \text{solid phase}, \\ \left.\begin{aligned} &T_l = T_s = T_0 - mC_l, \;\; C_s = kC_l, \\ &\lambda_s \mathbf{n}\nabla T_s - \lambda_l \mathbf{n}\nabla T_l = \rho L u, \\ &-m\mathbf{n}\nabla C_l = \mathbf{n}\nabla T_l \end{aligned}\right\} \text{discontinuity interface}. \end{gathered} \tag{9}$$

During the crystallization of a liquid with a mushy layer, the solidified material represents a heterogeneous mixture of volumes with solute concentration kC_{pi}, formed as a result of the phase transition at $y = 0$. They are directly adjacent to the liquid phase of the two-phase (mushy) layer with inclusions of solid phase elements that have developed in the two-phase region. The solute concentration in them is not homogeneous and is determined by the current value of solute concentration $C(y)$ in the mushy layer during their growth time. The topological features of this mixture are determined primarily by the mushy layer structure. Hence, the mushy layer crystallization process is fundamentally different from the frontal process when the solid material is microscopically homogeneous.

If we neglect diffusion in the solid phase and do not set the task in describing its detailed structure, then the concentration distribution in a mushy region becomes unnecessary. In this case, model (9) contains all the boundary conditions on the discontinuity interface required for the correct statement of the heat transfer problem in liquid and solid phases and the mass of dissolved impurity in the liquid phase, and also for finding the crystallization velocity u.

Let us consider below the steady-state and self-similar crystallization processes as examples illustrating the influence of the mushy layer on directional solidification. As this takes place, we consider the following simplifications of the solidification process throughout the paper: (i) local equilibrium conditions of directional crystallization when the impurity diffusion is described by a parabolic equation; (ii) a binary mixture when there are the main solidifying component and an impurity dissolved therein; (iii) crystallization with constant and self-similar (inversely proportional to the square root of time) velocities; (iv) no nucleation and bulk crystal growth in the two-phase region; (v) no convection in the liquid and two-phase regions.

3. Steady-State Crystallization

For simplicity of the analysis, let us consider the stationary crystallization mode with a planar discontinuity interface mimicking a mushy layer taking into account the fact that the temperature diffusivity coefficients in both the phases are several orders of magnitude greater than the diffusion coefficient in the liquid. This means that the relaxation time of the temperature field is much less than the relaxation time of concentration field, and, hence, the thermal conductivity equations can be approximated as stationary. In other words, here, we consider a rather slow process of directional crystallization with constant velocity u in the field of fixed temperature gradients. Neglecting the solid phase diffusion, we arrive at the following model in the moving reference frame:

$$\begin{aligned} T_l(y) &= T_0 - mC_{pi} + g_l y,\ y > 0, \\ T_s(y) &= T_0 - mC_{pi} + g_s y,\ y < 0, \\ u &= \frac{\lambda_s g_s - \lambda_l g_l}{\rho L}, \\ \frac{\partial C_l}{\partial \tau} - u\frac{\partial C_l}{\partial y} &= D_l \frac{\partial^2 C_l}{\partial y^2},\ y > 0, \\ C_l &\to C_\infty,\ \tau = 0 \text{ and } y \to \infty, \\ -D_l \frac{\partial C_l}{\partial y} &= (1-k)C_l u,\ y = 0, \text{ before CS}, \\ -m\frac{\partial C_l}{\partial y} &= g_l,\ y = 0, \text{ after CS}, \end{aligned} \tag{10}$$

where $\tau = t$ is time in the moving reference frame. Note that the last lines of (10) represent the boundary conditions for the solute concentration at the discontinuity interface $y = 0$. As this takes place, the first of them is valid at the initial process stages before the initiation of constitutional supercooling (CS) when the liquid–solid phase interface is planar. The second condition should be used immediately after the CS appearance when the liquid–solid phase

boundary is replaced by a discontinuity interface. Note that this model of directional solidification describes the Czochralski method of crystal pulling from the melt and experiments on the steady-state crystallization of binary mixtures (see, among others, [11,41–44]).

Let us first consider the first problem where crystallization occurs with a planar phase interface. Applying the integral Laplace transform to the corresponding concentration problem in (10), we obtain

$$\begin{aligned} sC_l^* - C_\infty - u\frac{dC_l^*}{dy} &= D_l\frac{d^2C_l^*}{dy^2},\ y>0,\\ -D_l\frac{dC_l^*}{dy} &= (1-k)C_l^*u,\ y=0,\ \ C_l^*\to\frac{C_\infty}{s},\ y\to\infty. \end{aligned} \tag{11}$$

Here, s represents the Laplace transform parameter, and the subscript $*$ designates the Laplace transform space.

The solution to the problem (11) reads as

$$\begin{aligned} C_l^*(y) = \frac{C_\infty}{s} &+ \frac{2(1-k)C_\infty}{s\left(\sqrt{1+\dfrac{4D_ls}{u^2}}+2k-1\right)}\\ &\times\exp\left[-\frac{u}{2D_l}\left(\sqrt{1+\frac{4D_ls}{u^2}}+1\right)y\right]. \end{aligned} \tag{12}$$

To find the inverse Laplace transform of expression (12), we use the following tabulated transform [45]:

$$\begin{aligned} \frac{\exp\left(-\sqrt{\alpha(s+\gamma)}\right)}{s(\beta+\sqrt{s+\gamma})} \to{}& \frac{\exp\left(-\sqrt{\alpha\gamma}\right)}{2(\beta+\sqrt{\gamma})}\operatorname{erfc}\left(\sqrt{\frac{\alpha}{4\tau}}-\sqrt{\gamma\tau}\right)\\ &+\frac{\exp\left(\sqrt{\alpha\gamma}\right)}{2(\beta-\sqrt{\gamma})}\operatorname{erfc}\left(\sqrt{\frac{\alpha}{4\tau}}+\sqrt{\gamma\tau}\right)\\ &-\frac{\beta\exp\left(\beta\sqrt{\alpha}+\beta^2\tau-\gamma\tau\right)}{\beta^2-\gamma}\operatorname{erfc}\left(\sqrt{\frac{\alpha}{4\tau}}+\beta\sqrt{\tau}\right) \end{aligned}$$

with

$$\alpha=\frac{y^2}{D_l},\ \ \beta=\frac{(2k-1)u}{2\sqrt{D_l}},\ \ \gamma=\frac{u^2}{4D_l}.$$

Also, taking $1/s\to 1$ into account, we obtain from (12) the solute concentration in real space:

$$\begin{aligned} C_l(y,\tau) = C_\infty\Bigg[1+\frac{1-k}{2k}N_1(y,\tau)\exp\left(-\frac{uy}{D_l}\right)-\frac{N_2(y,\tau)}{2}\\ +\frac{(2k-1)N_3(y,\tau)}{2k}\exp\left(\frac{(k-1)uy}{D_l}+\frac{k(k-1)u^2\tau}{D_l}\right)\Bigg], \end{aligned} \tag{13}$$

where

$$\begin{aligned} N_1(y,\tau) &= \operatorname{erfc}\left(\frac{y}{2\sqrt{D_l\tau}}-\frac{u}{2}\sqrt{\frac{\tau}{D_l}}\right),\\ N_2(y,\tau) &= \operatorname{erfc}\left(\frac{y}{2\sqrt{D_l\tau}}+\frac{u}{2}\sqrt{\frac{\tau}{D_l}}\right),\\ N_3(y,\tau) &= \operatorname{erfc}\left(\frac{y}{2\sqrt{D_l\tau}}+(2k-1)\frac{u}{2}\sqrt{\frac{\tau}{D_l}}\right). \end{aligned}$$

The distribution of solute concentration (13) in liquid takes place either (i) when no constitutional supercooling occurs at all and the crystallization process happens with a planar phase interface at all times or (ii) until the time of occurrence of constitutional supercooling (mushy layer) as long as the crystallization process happens with a planar phase interface.

Note that the nonstationary solute concentration given by expression (13) tends towards its steady-state profile (2) as $\tau \to \infty$. This can be easily shown by expanding (12) at $s \to 0$. This gives

$$C_l^*(y) = C_\infty \left[\frac{1}{s} + \frac{(1-k)}{ks} \exp\left(-\frac{uy}{D_l} \right) \right]. \tag{14}$$

The inverse Laplace transform of Equation (14) easily leads to the steady-state profile (2).

Now, substituting (13) into (4), we come to the following condition of constitutional supercooling incipience:

$$\begin{aligned} \Phi(\tau) \equiv \operatorname{erfc}\left(-\frac{u}{2}\sqrt{\frac{\tau}{D_l}} \right) + (2k-1) \exp\left(\frac{k(k-1)u^2\tau}{D_l} \right) \\ \times \operatorname{erfc}\left((2k-1)\frac{u}{2}\sqrt{\frac{\tau}{D_l}} \right) - \frac{2kD_l g_l}{(1-k)mC_\infty u} > 0. \end{aligned} \tag{15}$$

The time τ_* of constitutional supercooling (mushy layer) incipience can be found from the equality $\Phi(\tau_*) = 0$. If condition (15) is satisfied, the constitutional supercooling appears ahead of the planar phase interface, and the crystallization process is described by means of the model with discontinuity surface $y = 0$. In this case, the boundary condition at $y = 0$ should be changed (see the last line of model (10)). In the Laplace transform space, the boundary value problem looks like

$$\begin{aligned} sC_l^* - C_\infty - u\frac{dC_l^*}{dy} = D_l \frac{d^2 C_l^*}{dy^2},\ y > 0, \\ -m\frac{dC_l^*}{dy} = \frac{g_l}{s},\ y = 0;\ \ C_l^* \to \frac{C_\infty}{s},\ y \to \infty. \end{aligned} \tag{16}$$

Its solution reads as

$$\begin{aligned} C_l^*(y) = \frac{C_\infty}{s} + \frac{2D_l g_l C_\infty}{mC_\infty us\left(\sqrt{1 + \frac{4D_l s}{u^2}} + 1 \right)} \\ \times \exp\left[-\frac{u}{2D_l}\left(\sqrt{1 + \frac{4D_l s}{u^2}} + 1 \right) y \right]. \end{aligned} \tag{17}$$

Using the following tabulated Laplace transform [45],

$$\begin{aligned} \frac{\exp\left(-\sqrt{\alpha(s+\gamma)} \right)}{\beta + \sqrt{s+\gamma}} \to \exp(-\gamma\tau)\left[\frac{1}{\sqrt{\pi\tau}} \exp\left(-\frac{\alpha}{4\tau} \right) \right. \\ \left. -\beta \exp\left(\beta\sqrt{\alpha} + \beta^2\tau \right) \operatorname{erfc}\left(\sqrt{\frac{\alpha}{4\tau}} + \beta\sqrt{\tau} \right) \right] \end{aligned}$$

with $\beta = u/(2\sqrt{D_l})$ and the same values of α and γ, we obtain

$$C_l(y,\tau) = C_\infty \left[1 + \frac{\sqrt{D_l} g_l}{mC_\infty} \exp\left(-\frac{uy}{2D_l} \right) \int_0^\tau F(y,\tau_1) d\tau_1 \right], \tag{18}$$

$$F(y,\tau) = \frac{1}{\sqrt{\pi\tau}} \exp\left(-\frac{u^2\tau}{4D_l} - \frac{y^2}{4D_l\tau}\right)$$
$$-\frac{u}{2\sqrt{D_l}} \exp\left(\frac{uy}{2D_l}\right) \operatorname{erfc}\left(\frac{y}{2\sqrt{D_l\tau}} + \frac{u}{2}\sqrt{\frac{\tau}{D_l}}\right).$$

This concentration distribution takes place ahead of the discontinuity interface at $\tau > \tau_*$.

Figure 4 shows that the solute concentration distributions (13) (planar phase interface) and (18) (discontinuity interface representing the mushy layer) in liquid are very different. We demonstrate this discrepancy by the dotted and solid lines at the phase interface $y = 0$. The solute concentration found within the framework of mushy layer formation (discontinuity interface) can be essentially lower than the concentration corresponding to the planar phase interface (compare the dotted and solid lines). As this takes place, the difference between these solute concentrations increases with increasing crystallization velocity u. In addition, as the partition coefficient k decreases (Figure 4b), the difference in the solute distributions becomes larger and can reach several times the size when taking the mushy layer formation into consideration.

Generally speaking, three scenarios of directional crystallization can occur. (i) The constitutional supercooling condition (4) is not satisfied at all times, and the system crystallizes with a planar interface. (ii) Constitutional supercooling condition (4) is satisfied at a certain time $\tau = \tau_*$ so the binary liquid crystallizes with a planar interface at $\tau < \tau_*$ and a mushy layer (discontinuity interface) at $\tau \geq \tau_*$. (iii) Constitutional supercooling condition (4) is always satisfied at $\tau \geq 0$, and the system crystallizes with a mushy layer (discontinuity interface) at all times. The last crystallization scenario corresponds to curves (2) and (3) in Figure 4a. The rest curves illustrated in Figure 4a,b correspond to case (ii).

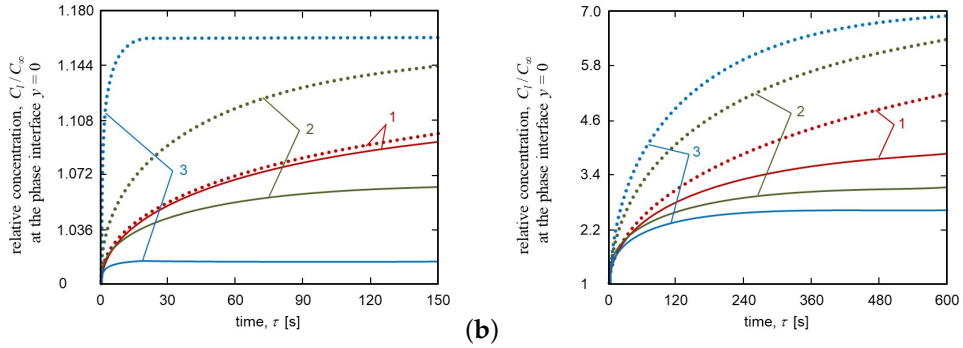

(**a**) (**b**)

Figure 4. Relative solute concentration at the phase interface as a function of time for Ti-Al (**a**) and Al-B (**b**) melts (material parameters are listed in Table 1). Dotted and solid lines are plotted accordingly to distributions (13) in the case of planar phase interface and (18) in the case of discontinuity interface (mushy layer), respectively. Numbers at the curves correspond to various crystallization velocities: (**a**) $u = 5 \times 10^{-6}$ m/s (1), $u = 10^{-5}$ m/s (2), $u = 5 \times 10^{-5}$ m/s (3) and $g_l = 6 \times 10^3$ K/m; (**b**) $u = 4 \times 10^{-6}$ m/s (1), $u = 6 \times 10^{-6}$ m/s (2), $u = 8 \times 10^{-6}$ m/s (3) and $g_l = 8 \times 10^4$ K/m. Constitutional supercooling appears ahead of the phase interface at (**a**) $\tau_* = 8$ s (1) and (**b**) $\tau_* = 241$ s (1), $\tau_* = 31$ s (2), $\tau_* = 6.2$ s (3). Crystallization occurs immediately with a mushy layer at $\tau \geq 0$ in panel (**a**) for curves (2) and (3).

Let us find the asymptotic concentration distribution at $\tau \to \infty$ when dealing with the mushy layer crystallization scenario. To easily perform this, we rewrite (17) at $s \to 0$ in the form of

$$C_l^*(y) = C_\infty \left[\frac{1}{s} + \frac{D_l g_l}{m C_\infty u s} \exp\left(-\frac{uy}{D_l}\right)\right]. \tag{19}$$

Applying the inverse Laplace transform to Equation (19), we have

$$C_l = C_\infty \left[1 + \frac{D_l g_l}{m C_\infty u} \exp\left(-\frac{uy}{D_l} \right) \right], \ y > 0, \ \tau \to \infty. \tag{20}$$

Comparing (2) and (20), we see that these distributions are similar, with various pre-exponential factors. In other words, the growth rate dC_l/dy of the solute concentration at $y = 0$ in the case of the planar phase interface (expression (2)) is $-(1-k)C_\infty u/(kD_l)$, whereas this rate for the discontinuity surface (expression (20)) equals $-g_l/m$. Obviously, this difference is due to the replacement of the actual mushy layer with a discontinuity interface with a boundary condition that takes into account the growth of solid phase elements and redistribution of solute concentration due to the appearance of constitutional supercooling.

4. Self-Similar Crystallization

Let us now consider a self-similar crystallization mode where the liquid and solid phases occupy the domains $\Sigma(\tau) < x < \infty$ and $-\infty < x < \Sigma(\tau)$, respectively. The planar phase interface (before the time τ_* of constitutional supercooling incipience) is between the liquid and solid phases at $x = \Sigma(\tau)$, playing the role of crystallization front. When the constitutional supercooling arises at τ_*, the liquid and solid phases are divided by a discontinuity interface $x = \Sigma(\tau)$ playing the role of mushy layer. The mathematical models describing these cases are very similar. The difference between them is only one boundary condition at $x = \Sigma(\tau)$. Namely, we have model (1) when considering the planar phase interface (at $\tau < \tau_*$) and model (9) when considering the discontinuity interface (at $\tau > \tau_*$). As before, we neglect diffusion in the solid material. Introducing the self-similar variables and dimensional parameters,

$$\begin{gathered} z = \frac{x}{2\sqrt{D_l \tau}}, \ \Sigma(\tau) = 2\delta\sqrt{D_l \tau}, \ \epsilon_l = \frac{D_l}{a_l}, \\ \epsilon_s = \frac{D_l}{a_s}, \ \Lambda = \frac{\lambda_s}{\lambda_l}, \ P = \frac{\rho L D_l}{\lambda_l T_0}, \end{gathered} \tag{21}$$

we arrive at the following heat and mass transfer problem:

$$\begin{gathered} \frac{d^2 T_l}{dz^2} = -2\epsilon_l z \frac{dT_l}{dz}, \ \frac{d^2 C_l}{dz^2} = -2z\frac{dC_l}{dz}, \ z > \delta, \\ \frac{d^2 T_s}{dz^2} = -2\epsilon_s z \frac{dT_s}{dz}, \ z < \delta, \\ T_l = T_s = T_0 - mC_l, \ \Lambda \frac{dT_s}{dz} - \frac{dT_l}{dz} = 2PT_0\delta, \ z = \delta, \\ T_l \to T_{l\infty}, \ C_l \to C_\infty, \ z \to \infty; \ \ T_s \to T_{s\infty}, \ z \to -\infty, \\ -\frac{dC_l}{dz} = 2(1-k)C_l\delta, \ z = \delta, \text{ before CS}, \\ -m\frac{dC_l}{dz} = \frac{dT_l}{dz}, \ z = \delta, \text{ after CS}. \end{gathered} \tag{22}$$

Here, the self-similar variable z takes spatial and time variables x and τ into account, the phase interface $\Sigma(\tau)$ is moving in a self-similar manner as a square root function of time τ and δ is the phase interface coordinate in self-similar variables (this parameter is a part of the solution to problem (22)). Note that this model of directional solidification describes the self-similar crystallization conditions establishing at large times (see, among others, [19,30,46]).

The solution to this problem reads as

$$\begin{gathered} T_l(z) = T_{l\infty} + A_l \mathrm{erfc}(\sqrt{\epsilon_l} z),\ C_l(z) = C_\infty + C\mathrm{erfc}(z),\ z > \delta, \\ T_s(z) = T_{s\infty} + A_s \mathrm{erfc}(-\sqrt{\epsilon_s} z),\ z < \delta, \\ A_l(\delta) = \frac{\sqrt{\pi} P T_0 \delta \mathrm{erfc}(-\sqrt{\epsilon_s}\delta) - \Lambda\sqrt{\epsilon_s}\exp\left(-\epsilon_s\delta^2\right)(T_{l\infty} - T_{s\infty})}{\sqrt{\epsilon_l}\exp(-\epsilon_l\delta^2)\mathrm{erfc}(-\sqrt{\epsilon_s}\delta) + \Lambda\sqrt{\epsilon_s}\exp(-\epsilon_s\delta^2)\mathrm{erfc}\left(\sqrt{\epsilon_l}\delta\right)}, \\ A_s(\delta) = \frac{T_{l\infty} - T_{s\infty} + A_l(\delta)\mathrm{erfc}\left(\sqrt{\epsilon_l}\delta\right)}{\mathrm{erfc}(-\sqrt{\epsilon_s}\delta)}, \\ C(\delta) = \frac{T_0 - T_{l\infty} - mC_\infty - A_l(\delta)\mathrm{erfc}\left(\sqrt{\epsilon_l}\delta\right)}{m\ \mathrm{erfc}(\delta)}. \end{gathered} \tag{23}$$

Here, parameter δ for the planar phase interface and discontinuity interface growth modes is defined as a root of transcendental equations

$$\begin{gathered} C(\delta)\exp\left(-\delta^2\right) - \sqrt{\pi}(1-k)\delta[C_\infty + C(\delta)\mathrm{erfc}(\delta)] = 0, \\ \text{planar phase interface before CS,} \\ A_l(\delta)\sqrt{\epsilon_l}\exp\left(-\epsilon_l\delta^2\right) + mC(\delta)\exp\left(-\delta^2\right) = 0, \\ \text{discontinuity interface after CS.} \end{gathered} \tag{24}$$

Figure 5 illustrates the solute concentration and temperature in the liquid and solid phases for both cases under consideration (solid lines demonstrate the solute concentration for a planar phase interface, while dotted lines show the concentration for the discontinuity interface mimicking a mushy layer). First of all, we can see that the liquid–solid interface moves faster in the case of mushy layer formation (compare the vertical green and red dashed lines). As this takes place, the solute concentrations in the liquid and solid phases become lower, while the temperatures in these phases become higher. Note that the difference between the concentration distributions increases as the heat removal into the solid phase increases (as the temperature $T_{s\infty}$ decreases). In addition, the presence of the mushy layer causes redistribution of impurity in the solid material due to mass transfer processes. Namely, the impurity displacement by the solid phase into interdendritic interstices and merging of branching dendrite-like structures can lead to the formation of impurity-rich liquid phase regions in the mushy layer and modify the structure and properties of a crystallized material.

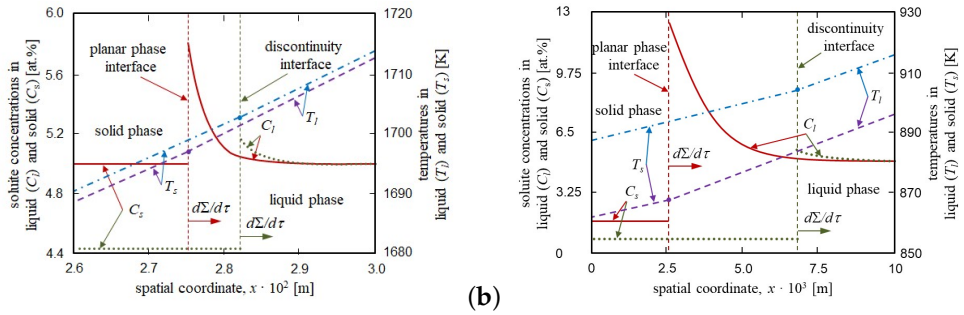

(**a**) (**b**)

Figure 5. Solute concentrations in liquid (C_l) and solid ($C_s = kC_l$) phases (scale of values on the left) and temperatures in liquid (T_l) and solid (T_s) phases (scale of values on the right) as functions of spatial coordinate x for Ti-Al (**a**) and Al-B (**b**) melts at $\tau = 600$ s (material parameters are listed in Table 1). The solid and dotted lines show the solute concentration for a planar phase interface ($\delta = 7.738$ (**a**) and $\delta = 0.802$ (**b**)) and discontinuity interface ($\delta = 7.933$ (**a**) and $\delta = 2.109$ (**b**)), respectively. The dashed and dash-dotted lines designate the temperature profiles for the planar phase interface and discontinuity interface, respectively. Vertical lines illustrate the planar phase interface ($\Sigma = 0.02752$ m (**a**) and $\Sigma = 0.00261$ m (**b**)) and a discontinuity interface ($\Sigma = 0.02821$ m (**a**) and $\Sigma = 0.00685$ m (**b**)).

Since accounting for all real heat and mass transfer processes leads to a strongly nonlinear, hardly analyzable model with a mushy layer, the simpler mathematical model with a discontinuity interface (reflecting the mushy layer) considered above provides a basis for theoretical description which can be fruitfully used for solving a number of specific problems. Let us especially highlight that the replacement of the real two-phase layer by a discontinuity interface allows all available research methods for analyzing the moving boundary problems (problems with a sharp crystallization front) to be applied to describe the phase transformation processes with a mushy layer. So, for example, the technique of morphological/dynamic stability analysis is used when selecting a stable growth regime and studying the formation of cellular and banded impurity structures arising due to the formation of stable and auto-oscillatory crystallization modes [47–49]. The technique of stochastic sensitivity analysis can be used to study the influence of atmospheric temperature and fluid velocity fluctuations [50,51]. The phase-field and enthalpy-based methods enable the analysis of various material properties and dynamic characteristics of crystallization phenomena with a sharp liquid–solid interface [52–55].

5. Conclusions

In summary, the influence of a two-phase (mushy) layer consisting of a mixture of solid and liquid phases on the directional crystallization process is considered. Such a layer arises due to the effect of constitutional supercooling appearing ahead of the liquid–solid phase interface as a result of impurity displacement by the growing solid material. A thin mushy layer is replaced by the discontinuity interface between liquid and solid phases that takes the temperature and solute concentration jumps into account. We analytically compare two mathematical models with a planar phase interface and discontinuity interface (mushy layer) and show that both of them have significant differences when a binary melt solidifies in the steady-state and self-similar manners. The main conclusion is that the solute distributions in liquid and solid phases may vary by several times when comparing a mushy layer and planar phase interface. Also, the temperature distributions, crystallization velocity and phase interface coordinate are very different in these two cases. This shows the necessity of taking into account the origin and development of a mushy layer in directional crystallization processes. Indeed, dendrite-like structures and the nucleation and enlargement of crystals, as well as redistribution of dissolved impurity, can occur simultaneously in such a layer. This, in turn, results in changes of the microstructure and properties of solid materials, velocity and time of the crystallization process.

Author Contributions: Conceptualization, D.V.A. and L.V.T.; methodology, D.V.A. and A.A.I.; software, D.V.A. and I.V.A.; validation, D.V.A. and L.V.T.; formal analysis, D.V.A., A.A.I. and L.V.T.; investigation, D.V.A.; resources, L.V.T.; writing—original draft preparation, D.V.A., I.V.A., A.A.I. and L.V.T.; writing—review and editing, D.V.A., I.V.A., A.A.I. and L.V.T.; visualization, I.V.A.; supervision, D.V.A.; project administration, D.V.A.; funding acquisition, D.V.A. All authors have read and agreed to the published version of the manuscript.

Funding: The theory under consideration was financially supported by the Russian Science Foundation (project no. 24-19-00566). For the computational algorithms development, L.V.T. gratefully acknowledges research funding from the Ministry of Science and Higher Education of the Russian Federation (project 075-02-2024-1428 for the development of the regional scientific and educational mathematical center "Ural Mathematical Center").

Data Availability Statement: All data generated or analyzed during this study are included in this published article.

Conflicts of Interest: The authors declare no conflicts of interest.

Abbreviations

Latin symbols

a	Temperature diffusivity, $m^2\ s^{-1}$
C	Solute concentration, at.%
C_∞	Solute concentration in liquid at infinity, at.%
D	Diffusion coefficient, $m^2\ s^{-1}$
g	Temperature gradient, $K\ m^{-1}$
h	Thickness of the supercooled layer, m
k	Equilibrium partition coefficient, -
L	Latent heat parameter, $J\ kg^{-1}$
m	Equilibrium liquidus slope, $K\ at.\%^{-1}$
$\mathbf{n}$	Normal vector to the phase interface, -
t	Time, s
T	Temperature, K
T_0	Crystallization temperature of pure melt, K
$T_{l\infty}$	Far-field temperature in liquid, K
$T_{s\infty}$	Far-field temperature in solid, K
u	Crystallization velocity, $m\ s^{-1}$
x	Spatial coordinate, m
y	Spatial coordinate, m
z	Self-similar variable, -

Greek symbols

δ	Phase interface coordinate in self-similar variables, -
λ	Thermal conductivity, $J\ s^{-1}\ K^{-1}\ m^{-1}$
ρ	Density of solid phase, $kg\ m^{-3}$
τ	Time, s
Σ	Liquid–solid phase interface coordinate, m

Abbreviations

l	Liquid phase
s	Solid phase
pi	Phase interface

References

1. Meirmanov, A.M. *The Stefan Problem*; W. De Gruyter Expositions in Mathematics; De Gruyter: Berlin, Germnay, 1992.
2. Buyevich, Y.A.; Alexandrov, D.V.; Mansurov, V.V. *Macrokinetics of Crystallization*; Begell House: New York, NY, USA, 2001.
3. Ivantsov, G.P. Diffusive supercooling in binary alloy solidification. *Dokl. Akad. Nauk SSSR* **1951**, *81*, 179–182.
4. Galenko, P.K.; Toropova, L.V.; Alexandrov, D.V.; Phanikumar, G.; Assadi, H.; Reinartz, M.; Paul, P.; Fang, Y.; Lippmann, S. Anomalous kinetics, patterns formation in recalescence, and final microstructure of rapidly solidified Al-rich Al-Ni alloys. *Acta Mater.* **2022**, *241*, 118384. [CrossRef]
5. Reinartz, M.; Kolbe, M.; Herlach, D.M.; Rettenmayr, M.; Toropova, L.V.; Alexandrov, D.V.; Galenko, P.K. Study on anomalous rapid solidification of Al-35 at%Ni in microgravity. *JOM* **2022**, *74*, 2420–2427. [CrossRef]
6. Toropova, L.V.; Alexandrov, D.V. Dynamical law of the phase interface motion in the presence of crystals nucleation. *Sci. Rep.* **2022**, *12*, 10997. [CrossRef] [PubMed]
7. Alexandrov, D.V.; Toropova, L.V. The role of incoming flow on crystallization of undercooled liquids with a two-phase layer. *Sci. Rep.* **2022**, *12*, 17857. [CrossRef] [PubMed]
8. Kurz, W.; Fisher, D.J. *Fundamentals of Solidification*; Trans. Tech. Publ.: Aedermannsdorf, Switzerland, 1989.
9. Vabishchevich, P.N.; Mansurov, V.V.; Churbanov, A.G. Numerical simulation of crystallization from a melt with consideration of impurity redistribution. *Russ. Chem. Ind.* **1994**, *26*, 54–70.
10. Alexandrova, I.V.; Alexandrov, D.V.; Aseev, D.L.; Bulitcheva, S.V. Mushy layer formation during solidification of binary alloys from a cooled wall: The role of boundary conditions. *Acta Phys. Pol. A* **2009**, *115*, 791–794. [CrossRef]
11. Peppin, S.S.L.; Aussillous, P.; Huppert, H.E.; Worster, M.G. Steady-state mushy layers: Experiments and theory. *J. Fluid Mech.* **2007**, *570*, 69–77. [CrossRef]
12. Buyevich, Y.A.; Alexandrov, D.V. *Heat Transfer in Dispersions*; Begell House: New York, NY, USA, 2005.

13. Lifshitz, E.M.; Pitaevskii, L.P. *Physical Kinetics*; Pergamon: Oxford, UK, 1981.
14. Alexandrov, D.V.; Makoveeva, E.V.; Ivanov, A.A.; Alexandrova, I.V. Desupersaturation dynamics in solutions with applications to bovine and porcine insulin crystallization. *J. Phys. A Math. Theor.* **2023**, *56*, 455702.
15. Alexandrov, D.V.; Dubovoi, G.Y.; Malygin, A.P.; Nizovtseva, I.G.; Toropova, L.V. Solidification of ternary systems with a nonlinear phase diagram. *Russ. Metall.* **2017**, *2017*, 127–135. [CrossRef]
16. Makoveeva, E.V.; Alexandrov, D.V. An exact solution to nonstationary Smoluchowski's coagulation equation complicated by Ostwald ripening. *Int. J. Heat Mass Trans.* **2023**, *217*, 124706. [CrossRef]
17. Hills, R.N.; Loper, D.E.; Roberts, P.H. A thermodynamically consistent model of a mushy zone. *Q. J. Mech. Appl. Mech.* **1983**, *36*, 505–539. [CrossRef]
18. Fowler, A.C. The formation of freckles in binary alloys. *IMA J. Appl. Math.* **1985**, *35*, 159–174. [CrossRef]
19. Worster, M.G. Solidification of an alloy from a cooled boundarys. *J. Fluid Mech.* **1986**, *167*, 481–501. [CrossRef]
20. Alexandrov, D.V.; Ivanov, A.A. The Stefan problem of solidification of ternary systems in the presence of moving phase transition regions. *J. Exper. Theor. Phys.* **2009**, *108*, 821–829. [CrossRef]
21. Makoveeva, E.V. Steady-state crystallization with a mushy layer: A test of theory with experiments. *Eur. Phys. J. Spec. Top.* **2023**, *232*, 1165–1169. [CrossRef]
22. Yoshizaki, I.; Ishikawa, T.; Adachi, S.; Yokoyama, E.; Furukawa, Y. Precise measurements of dendrite growth of ice crystals in microgravity. *Microgravity Sci. Technol.* **2012**, *24*, 245–253. [CrossRef]
23. Shibkov, A.A.; Zheltov, M.A.; Korolev, A.A.; Kazakov, A.A.; Leonov, A.A. Crossover from diffusion-limited to kinetics-limited growth of ice crystals. *J. Cryst. Growth* **2005**, *285*, 215–227. [CrossRef]
24. Yokoyama, E.; Yoshizaki, I.; Shimaoka, T.; Sone, T.; Kiyota, T.; Furukawa, Y. Measurements of growth rates of an ice crystal from supercooled heavy water under microgravity conditions: Basal face growth rate and tip velocity of a dendrite. *J. Phys. Chem. B* **2011**, *115*, 8739–8745. [CrossRef]
25. Alexandrov, D.V.; Titova, E.A.; Galenko, P.K.; Rettenmayr, M.; Toropova, L.V. Dendrite tips as elliptical paraboloids. *J. Phys. Condens. Matter* **2021**, *33*, 443002. [CrossRef]
26. Toropova, L.V. Shape functions for dendrite tips of SCN and Si. *Eur. Phys. J. Spec. Top.* **2022**, *231*, 1129–1133. [CrossRef]
27. Alexandrov, D.V. Solidification with a quasiequilibrium mushy region: Exact analytical solution of nonlinear model. *J. Cryst. Growth* **2001**, *222*, 816–821. [CrossRef]
28. Toropova, L.V.; Ivanov, A.A.; Osipov, S.I.; Yang, Y.; Makoveeva, E.V.; Alexandrov, D.V. Solidification of ternary melts with a two-phase layer. *J. Phys. Condens. Matter* **2022**, *34*, 383002. [CrossRef] [PubMed]
29. Aitta, A.; Huppert, H.E.; Worster, M.G. Diffusion-controlled solidification of a ternary melt from a cooled boundary. *J. Fluid Mech.* **2001**, *432*, 201–217. [CrossRef]
30. Anderson, D.M. A model for diffusion-controlled solidification of ternary alloys in mushy layers. *J. Fluid Mech.* **2003**, *483*, 165–197. [CrossRef]
31. Thomson, A.F.; Huppert, H.E.; Worster, M.G.; Aitta, A. Solidification and compositional convection of a ternary alloy. *J. Fluid Mech.* **2003**, *497*, 167–199. [CrossRef]
32. Mansurov, V.V. The nonlinear dynamics of solidification of a binary melt with a nonequilibrium mushy region. *Math. Comput. Modell.* **1990**, *14*, 819–821. [CrossRef]
33. Aseev, D.L.; Alexandrov, D.V. Directional solidification of binary melts with a non-equilibrium mushy layer. *Int. J. Heat Mass Trans.* **2006**, *49*, 4903–4909. [CrossRef]
34. Huguet, L.; Alboussière, T.; Bergman, M.I.; Deguen, R.; Labrosse, S.; Lesœur, G. Structure of a mushy layer under hypergravity with implications for Earth's inner core. *Geophys. J. Int.* **2016**, *204*, 1729–1755. [CrossRef]
35. Alexandrov, D.V.; Alexandrova, I.V.; Nikishina, M.A.; Malygin, A.P.; Toropova, L.V. Directional crystallization in the presence of a mushy layer with applications to the Earth's inner core boundary. *Crystals* **2023**, *13*, 1361. [CrossRef]
36. Hartmann, H.; Galenko, P.K.; Holland-Moritz, D.; Kolbe, M.; Herlach, D.M.; Shuleshova, O. Nonequilibrium solidification in undercooled $Ti_{45}Al_{55}$ melts. *J. Appl. Phys.* **2008**, *103*, 073509. [CrossRef]
37. Egry, I.; Brooks, R.; Holland-Moritz, D.; Novakovic, R.; Matsushita, T.; Ricci, E.; Seetharaman, S.; Wunderlich, R.; Jarvis, D. Thermophysical properties of γ-titanium aluminide: The European IMPRESS Project. *Int. J. Thermophys.* **2007**, *28*, 1026–1036. [CrossRef]
38. Galenko, P.K.; Reuther, K.; Kazak, O.V.; Alexandrov, D.V.; Rettenmayr, M. Effect of convective transport on dendritic crystal growth from pure and alloy melts. *Appl. Phys. Lett.* **2017**, *111*, 031602. [CrossRef]
39. Leitner, M.; Leitner, T.; Schmon, A.; Aziz, K.; Pottlacher, G. Thermophysical properties of liquid aluminum. *Metall. Mater. Trans. A* **2017**, *48*, 3036–3045. [CrossRef]
40. Aluminium/Aluminum Boron Master Alloy. AZO Materials. Available online: https://www.azom.com/article.aspx?ArticleID=7869 (accessed on 5 June 2024).
41. Flemings, M. *Solidification Processing*; McGraw Hill: New York, NY, USA, 1974.
42. Borisov, V.T. *Theory of Two-Phase Zone of Metallic Ingot*; Metallurgia: Moscow, Ruassia, 1987.
43. Czapelski, M. Variable equilibrium partition coefficient. *J. Cryst. Growth* **1998**, *187*, 138–139. [CrossRef]
44. Peppin, S.S.L.; Huppert, H.E.; Worster, M.G. Steady-state solidification of aqueous ammonium chloride. *J. Fluid Mech.* **2008**, *599*, 465–476. [CrossRef]

45. Ditkin, V.A.; Prudnikov, A.P. *Integral Transforms and Operational Calculus*; Pergamon: Oxford, UK, 1965.
46. Huppert, H.E.; Worster, M.G. Dynamic solidification of a binary melt. *Nature* **1985**, *314*, 703–707. [CrossRef]
47. Karma, A.; Sarkissian, A. Dynamics of banded structure formation in rapid solidification. *Phys. Rev. Lett.* **1992**, *68*, 2616–2619. [CrossRef]
48. Galenko, P.K.; Danilov, D.A. Selection of the dynamically stable regime of rapid solidification front motion in an isothermal binary alloy. *J. Cryst. Growth* **2020**, *216*, 512–526. [CrossRef]
49. Wang, H.; Liu, F.; Wang, K.; Zhai, H. Oscillatory morphological stability for rapid directional solidification: Effect of non-linear liquidus and solidus. *Acta Mater.* **2011**, *59*, 5859–5867. [CrossRef]
50. Makoveeva, E.V.; Alexandrov, D.V.; Bashkirtseva, I.A.; Ryashko, L.V. Sea ice freezes faster when fluctuations in the atmospheric temperature and friction velocity occur. *Eur. Phys. J. Spec. Top.* **2023**, *232*, 1153–1163. [CrossRef]
51. Alexandrov, D.V.; Bashkirtseva, I.A.; Malygin, A.P.; Ryashko, L.B. Sea ice dynamics induced by external stochastic fluctuations. *Pure Appl. Geophys.* **2013**, *170*, 2273–2282. [CrossRef]
52. Toropova, L.V.; Galenko, P.K.; Alexandrov, D.V.; Rettenmayr, M.; Kao, A.; Demange, G. Non-axisymmetric growth of dendrite with arbitrary symmetry in two and three dimensions: Sharp interface model vs. phase-field model. *Eur. Phys. J. Spec. Top.* **2020**, *229*, 2899–2909. [CrossRef]
53. Galenko, P.K. Phase-field model with relaxation of the diffusion flux in nonequilibrium solidification of a binary system. *Phys. Lett. A* **2001**, *287*, 190–197. [CrossRef]
54. Nizovtseva, I.G.; Galenko, P.K. Travelling-wave amplitudes as solutions of the phase-field crystal equation. *Phil. Trans. R. Soc. A* **2018**, *386*, 20170202. [CrossRef]
55. Kao, A.; Pericleous, K. A numerical model coupling thermoelectricity, magnetohydrodynamics and dendritic growth. *J. Algorithms Comput. Technol.* **2012**, *6*, 173–201. [CrossRef]